Mixed Metal Oxides

DOI: 10.1002/anie.201409776

Self-Templated Formation of Uniform $NiCo_2O_4$ Hollow Spheres with Complex Interior Structures for Lithium-Ion Batteries and Supercapacitors

*Laifa Shen, Le Yu, Xin-Yao Yu, Xiaogang Zhang, and Xiong Wen (David) Lou**

Abstract: *Despite the significant advancement in preparing metal oxide hollow structures, most approaches rely on template-based multistep procedures for tailoring the interior structure. In this work, we develop a new generally applicable strategy toward the synthesis of mixed-metal-oxide complex hollow spheres. Starting with metal glycerate solid spheres, we show that subsequent thermal annealing in air leads to the formation of complex hollow spheres of the resulting metal oxide. We demonstrate the concept by synthesizing highly uniform $NiCo_2O_4$ hollow spheres with a complex interior structure. With the small primary building nanoparticles, high structural integrity, complex interior architectures, and enlarged surface area, these unique $NiCo_2O_4$ hollow spheres exhibit superior electrochemical performances as advanced electrode materials for both lithium-ion batteries and supercapacitors. This approach can be an efficient self-templated strategy for the preparation of mixed-metal-oxide hollow spheres with complex interior structures and functionalities.*

Owing to their unique structural features in terms of low density, hollow interior, and shell permeability, hollow micro-/nanostructures have been attracting tremendous interest in various areas including catalysis, drug delivery, chemical sensors, energy conversion, energy storage systems, and many others.[1–9] In this context, intensive efforts have been devoted to developing different strategies for synthesizing hollow structures, which resulted in great progress in preparing many hollow structures such as hollow spheres,[10,11] boxes,[12,13] and micro-/nanotubes.[14,15] However, most of the available hollow structures possess relatively simple configurations, such as single-shelled hollow spheres of one composition. Researchers are currently more focused on the design and fabrication of hollow structures with higher complexity in terms of structure and composition, hoping to achieve optimized physical/chemical properties for specific applications. As a result, many types of hollow structures with multishelled architectures have been fabricated through different synthesis routes.[16–19] For example, Wang et al. reported the synthesis of multishelled Co_3O_4 hollow microspheres with carbonaceous microspheres as hard templates, which exhibit higher lithium storage capacity and improved cycling performance compared with single-shelled Co_3O_4 microspheres.[20] We have recently developed a new "penetration–solidification–annealing" strategy to fabricate various mixed-metal-oxide multishelled hollow spheres using carbon spheres as hard templates.[21] Several different types of Cu_2O multilevel hollow spheres are synthesized using different methods such as soft templating and Ostwald ripening process and their gas-sensing properties are investigated.[22,23] Despite the progress achieved to date, the current methods are mostly based on hard templates and are usually time-consuming and quite tedious because of the need for template synthesis and the multistep process. In addition, it is difficult to fabricate multicomponent metal oxide hollow structures because different materials with distinct physical/chemical properties could hardly be incorporated simultaneously during the synthesis process. Therefore, it is still desirable yet challenging to develop new efficient strategies to fabricate high-quality complex hollow structures, especially for multicomponent materials.

Transition metal oxides (TMOs), as an important class of functional materials, have been extensively studied as electrode materials for energy storage devices including fuel cells, lithium-ion batteries (LIBs), and electrochemical capacitors (ECs).[21,24–29] Ternary metal oxides with two different metal cations exhibit high electrochemical activities because of their complex chemical composition and the synergic effects of multiple metal species.[30,31] For example, spinel nickel cobaltite ($NiCo_2O_4$), in which one Co atom is replaced by Ni, possesses much better electrical conductivity and higher electrochemical activity than nickel oxides or cobalt oxides.[32,33] As a result, $NiCo_2O_4$ exhibits exceptionally high specific capacity/capacitance, which is typically 2–3 times higher than that of corresponding monometal oxides.

Herein, we have developed a new and generally applicable strategy for the efficient synthesis of mixed-metal-oxide hollow spheres with complex interior structures. The method involves the solution synthesis of uniform metal glycerate solid spheres and subsequent thermal annealing in air. We demonstrate the concept by synthesizing highly uniform $NiCo_2O_4$ hollow spheres with a core-in-double-shell interior structure. When evaluated as electrode materials for LIBs and ECs, these $NiCo_2O_4$ complex hollow spheres show high

[*] L. F. Shen, L. Yu, Dr. X. Y. Yu, Prof. X. W. Lou
School of Chemical and Biomedical Engineering
Nanyang Technological University
62 Nanyang Drive, Singapore 637459 (Singapore)
E-mail: xwlou@ntu.edu.sg
davidlou88@gmail.com
Homepage: http://www.ntu.edu.sg/home/xwlou/
L. F. Shen, Prof. X. G. Zhang
Jiangsu Key Laboratory of Material and Technology for Energy Conversion, College of Material Science and Engineering, Nanjing University of Aeronautics and Astronautics
Nanjing, 210016 (P.R. China)

Supporting information for this article is available on the WWW under http://dx.doi.org/10.1002/anie.201409776.

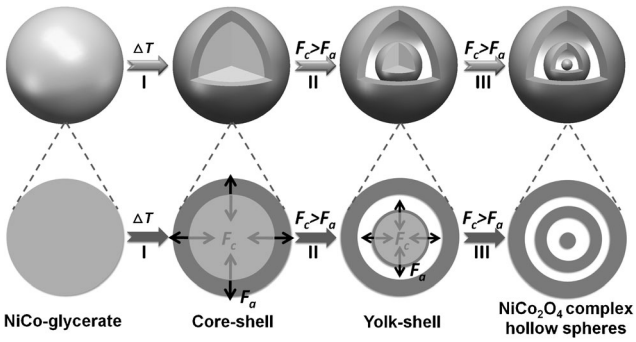

Figure 1. Schematic illustration of the formation process of $NiCo_2O_4$ core-in-double-shell hollow spheres.

capacity/capacitance, good cycling stability, and excellent rate performance.

Our strategy for the formation of mixed-metal-oxide complex hollow structures is shown in Figure 1, using $NiCo_2O_4$ as an example (the experimental details are provided in the Supporting Information, SI). In the first step, uniform nickel–cobalt glycerate (NiCo-glycerate) spheres as the precursor (Figure S1 A, SI) are prepared by a facile solvothermal method. The NiCo-glycerate solid spheres can be easily converted to $NiCo_2O_4$ core-in-double-shell hollow spheres by a simple nonequilibrium heat treatment process. Transmission electron microscopy (TEM) and powder X-ray diffraction (XRD) are conducted to monitor the morphological evolution and crystallization process after different thermal treatment durations. At the initial stage of calcination (stage I), the large temperature gradient (ΔT) existing along the radial direction leads to the quick formation of a $NiCo_2O_4$ shell on the surface of NiCo-glycerate spheres (Figure S1 B). Several weak diffraction peaks in the corresponding XRD pattern (Figure S2 A) can be indexed to the crystal planes of $NiCo_2O_4$. Thereafter, there are two actions in opposing directions acting on the interface between the $NiCo_2O_4$ shell and the NiCo-glycerate core (namely, heterogeneous contraction). One is the contraction (F_c) induced by the weight loss of around 46.9 % during the oxidative degradation of the organic species (Figure S3), resulting in inward shrinkage of the NiCo-glycerate core. The other is the adhesion action (F_a) from the relatively rigid shell, which hinders the inward contraction of the precursor core. When F_c is dominant (stage II), the inner core will further contract inward and detach from the preformed outer metal oxide shell, as confirmed by TEM image (Figure S1 C). The increase of diffraction peak intensity implies the growth of crystalline $NiCo_2O_4$ (Figure S2 B). With prolonged heating, the heterogeneous contraction process takes place on the interior core. By the same mechanism, the second shell is formed, producing a unique core-in-double-shell interior structure (Figure S1 D).

There is a pronounced diffraction peak at around 10° in the XRD pattern of NiCo-glycerate (Figure S4 A), which is characteristic of metal alkoxides.[34] After thermal treatment, all diffraction peaks of the product can be indexed to the cubic spinel $NiCo_2O_4$ phase (JCPDS card No. 20-0781; Figure S4 B). No residues or other phases are detected, indicating that the NiCo-glycerate is completely converted to spinel $NiCo_2O_4$ after a simple annealing process. The Ni/Co atomic ratio analyzed by energy-dispersive X-ray spectroscopy (EDX) analysis is about 0.5 (Figure S5).

The morphology and microstructure of the products are examined with field-emission scanning electron microscopy (FESEM) and TEM. As shown in Figure 2 A (also see

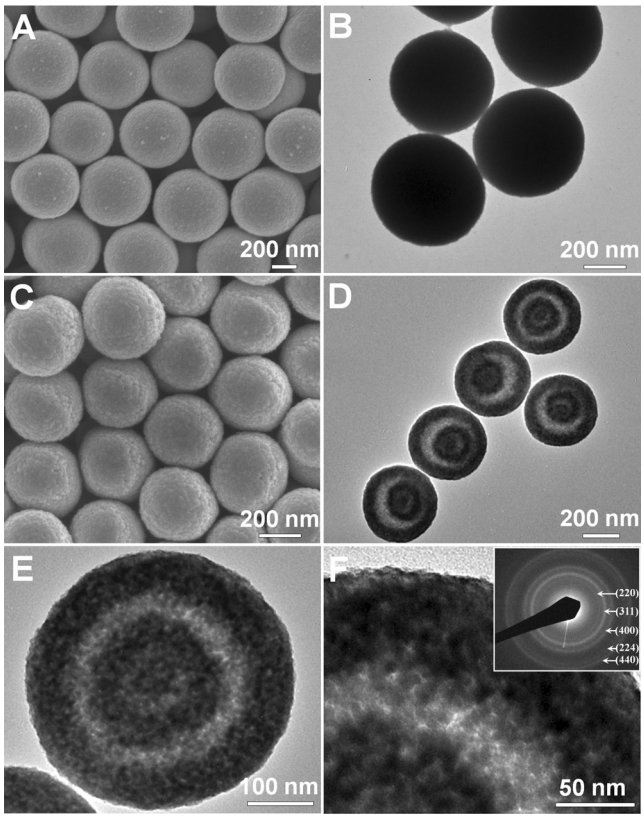

Figure 2. Typical FESEM (A, C) and TEM (B, D–F) images of the NiCo-glycolate precursor spheres (A, B) and $NiCo_2O_4$ core-in-double-shell hollow spheres (C–F). Inset in (F) shows the corresponding SAED pattern.

Figure S6 A), the NiCo-glycerate precursor spheres are highly uniform with relatively smooth surface and the diameter is around 550 nm. The TEM image (Figure 2 B) shows that these NiCo-glycerate spheres are completely solid spheres. After the thermal treatment, the NiCo-glycerate precursor is converted into spinel $NiCo_2O_4$, but the morphology (Figure S6 B) is perfectly preserved as highly uniform spheres. However the diameter of $NiCo_2O_4$ spheres is only about 400 nm (Figure 2 C,D), which is significantly smaller than that of NiCo-glycerate precursor spheres because of the shrinkage during calcination. Besides, the surface of the $NiCo_2O_4$ spheres is very rough, indicating that the spheres consist of small nanoparticles. The interior structure of the spheres is investigated by TEM. From the TEM images (Figure 2 D,E), it can be clearly observed that the $NiCo_2O_4$ spheres possess a three-layer core-in-double-shell hollow structure. The average diameters of the outer and inner shells as well as the solid core are about 400, 200, and 40 nm,

respectively, as estimated from the TEM images. In addition, the outer shell is relatively thick, with an average thickness of around 70 nm, whereas the inner shell is about 40 nm in thickness. The enlarged TEM image (Figure 2F) clearly shows that the shell is composed of small nanocrystals with interparticle mesopores distributed throughout the shell. As determined by N_2 sorption measurement (Figure S7), these $NiCo_2O_4$ complex hollow spheres possess a relatively high Brunauer–Emmett–Teller (BET) surface area of 61.2 $m^2 g^{-1}$ with pore sizes mostly below 10 nm. The selected-area electron diffraction (SAED) pattern of $NiCo_2O_4$ hollow spheres (inset in Figure 2F) clearly shows the polycrystalline nature of the sample and the diffraction rings can be readily indexed to the spinel $NiCo_2O_4$ phase.

The interior structure can be simply modulated by adjusting the heating rate during the calcination process (Figure S8). Specifically, core–shell spheres are obtained with a heating rate of 2 °C min^{-1} (Figure S8A). With a higher heating rate of 5 °C min^{-1}, the product still shows a core–shell structure (Figure S8B), but the diameters of the shell and inner solid core are about 360 and 250 nm, respectively, and the shell thickness decreases to only around 35 nm. When further the heating rate is further increased to 10 °C min^{-1}, the product is composed of porous solid spheres with a diameter of about 320 nm (Figure S8C). These results show that the heating rate plays an important role in the formation of complex interior structures.

Importantly, the present approach is simple and potentially general. We have successfully synthesized other mixed-metal-oxide hollow spheres with complex interior structures. For example, uniform ZnCo-glycerate spheres with a diameter of around 500 nm can be synthesized by a similar solvothermal method (Figure S9). After annealing treatment, ZnCo-glycerate is completely converted to spinel $ZnCo_2O_4$ with a large weight loss of around 47.1% (Figure S10). The spherical morphology is perfectly retained (Figure S11). The complex interior structure of the obtained $ZnCo_2O_4$ spheres can be clearly shown by TEM images (Figure S11C,D). Although the outer shell is close to the inner shell, a clear gap between them is still observed. This method is further extended to synthesize Mn-based mixed-metal-oxide hollow spheres. For example, CoMn-glycerate spheres with a diameter of around 1.5 μm were successfully synthesized (Figure S12A,B). After annealing treatment, CoMn-glycerate is completely converted to spinel $CoMn_2O_4$. FESEM and TEM images (Figure S12C,D) show that the morphology is well retained and the formed $CoMn_2O_4$ spheres have a yolk-shell interior structure with a porous/hollow yolk. The interior structures are slightly different for different metal oxides. This can be easily understood by considering the different crystallization and crystal growth behavior of different materials during the annealing process. As a result, the contraction and adhesion actions involved are different for different materials, hence producing different interior structures.

Mixed metal oxides have been regarded as a promising class of electrode materials for high-performance energy storage devices. The lithium storage properties of $NiCo_2O_4$ hollow spheres are evaluated by both cyclic voltammetry and galvanostatic charge–discharge cycling. Cyclic voltammograms (CVs) are obtained at a scan rate of 0.2 mV s^{-1} in the voltage window of 0.01–3 V versus Li/Li^+ (Figure S13). In the first cathodic sweep, the sharp peak at 0.67 V is attributed to the reduction of Co^{3+} and Ni^{2+} to metallic Co and Ni, respectively. Meanwhile, two poorly defined anodic peaks centered at about 1.58 and 2.22 V in the following anodic scan can be ascribed to the oxidation of metallic Ni and Co to NiO_x and CoO_x, respectively.[35] In the subsequent scans, the cathodic peak shifts to 0.91 V with reduced intensity. Figure 3A shows the charge–discharge voltage profiles of the

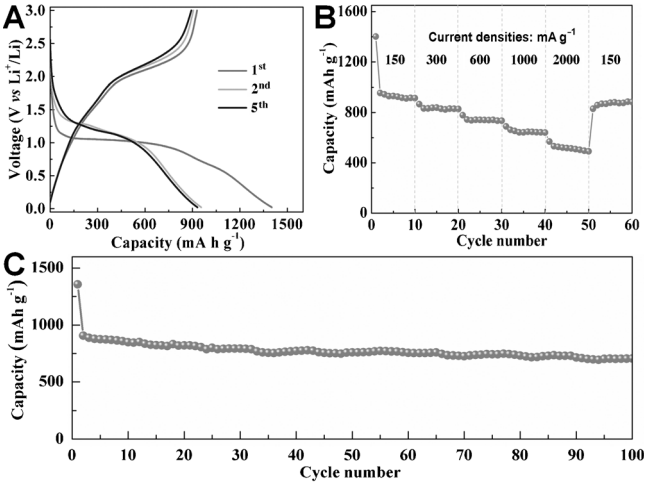

Figure 3. Electrochemical evaluation of $NiCo_2O_4$ hollow spheres for lithium-ion batteries: A) discharge–charge voltage profiles at a current density of 150 mA g^{-1}; B) rate capability at different current densities between 0.01 and 3.0 V; C) cycling performance at a current density of 200 mA g^{-1}.

$NiCo_2O_4$ hollow spheres at a current density of 150 mA g^{-1}. The $NiCo_2O_4$ electrode delivers high first-cycle discharge and charge capacities of 1401 and 928 mAh g^{-1} respectively, corresponding to a moderate irreversible loss of about 34%. The discharge–charge curves for the second and fifth cycles almost coincide with each other, indicating the good cycling stability. The rate capability is evaluated at different current densities ranging from 150 to 2000 mA g^{-1} (Figure 3B). As can be seen, the specific capacities are 834, 745, 662, and 533 mAh g^{-1} at the current densities of 300, 600, 1000, and 2000 mA g^{-1}, respectively. When the current density is changed back to 150 mA g^{-1} after 50 cycles, the reversible capacity resumes to 885 mAh g^{-1}. Furthermore, the $NiCo_2O_4$ hollow spheres electrode possesses excellent cyclic stability (Figure 3C). After continuous cycling for 100 cycles at a current density of 200 mA g^{-1}, a reversible discharge capacity as high as 706 mAh g^{-1} is retained, corresponding to 78% of the second-cycle discharge capacity. The lithium storage properties achieved in the present study are superior to that of many other different $NiCo_2O_4$ materials, including flower-like $NiCo_2O_4$,[36] $NiCo_2O_4$ microspheres,[37] $NiCo_2O_4$/C nanocomposites,[35] and $NiCo_2O_4$–RGO composite[38] (Table S1, SI). Clearly, the unique structure of present $NiCo_2O_4$ complex hollow structures is beneficial for enhanced

lithium storage properties. Specifically, the presence of small primary nanoparticles and pores can boost Li^+-ion transport, resulting in high capacity and excellent rate capability. More importantly, the unique three-layer core-in-double-shell interior structure could buffer the large volume change associated with the repeated Li^+ insertion/extraction processes during cycling and endow the structural integrity, thus alleviating the pulverization problem and enhancing the cycling stability.

In addition, the $NiCo_2O_4$ hollow spheres are also evaluated as an electrode material for ECs. Figure 4A gives

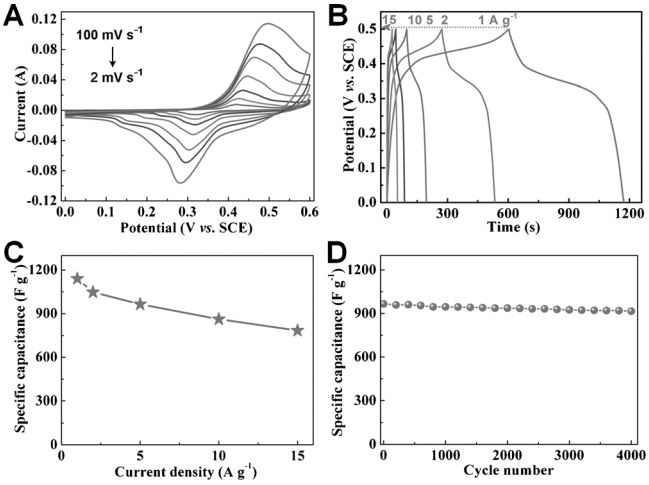

Figure 4. Electrochemical evaluation of $NiCo_2O_4$ hollow spheres for electrochemical capacitors: A) CV curves at 100, 60, 40, 20, 10, 5, and 2 $mV s^{-1}$, and B) galvanostatic charge–discharge voltage profiles at 15, 10, 5, 2, and 1 $A g^{-1}$. C) Specific capacitance as a function of current density calculated from discharge curves in (B). D) Cycling performance of the $NiCo_2O_4$ electrode at a current density of 5 $A g^{-1}$.

typical CV curves of the $NiCo_2O_4$ hollow spheres electrode with various sweep rates. A pair of well-defined redox peaks can be observed within the potential range from 0 to 0.6 V versus saturated calomel electrode (SCE) at all sweep rates, which is mainly attributed to the Faradaic redox reactions related to M–O/M–O–OH (M represents Ni or Co).[33] With the 50-fold increment in sweep rate from 2 to 100 $mV s^{-1}$, the position of the cathodic peak shifts slightly from 0.32 to 0.28 V, demonstrating that the $NiCo_2O_4$ electrode is favorable for ultrafast redox reactions. Figure 4B presents the galvanostatic charge–discharge voltage curves of the $NiCo_2O_4$ electrode at different current densities ranging from 1 to 15 $A g^{-1}$. Evidently, it can be observed that there are voltage plateaus at around 0.4 V, which is consistent with the above CV results. The calculated specific capacitance as a function of the discharge current density is plotted in Figure 4C. The $NiCo_2O_4$ electrode delivers high pseudocapacitance of 1141, 1048, 965, 862, and 784 $F g^{-1}$ at current densities of 1, 2, 5, 10, and 15 $A g^{-1}$, respectively. The results suggest that the $NiCo_2O_4$ hollow spheres electrode has excellent high-rate capability, compared with most $NiCo_2O_4$ electrodes reported in the literature.[39–42] This superior performance should be related to the advantageous structural features of these $NiCo_2O_4$ hollow spheres. Specifically, the shells consisting of small nanocrystals possess high porosity, and thus the electrolyte can easily penetrate through the shells for efficient redox reactions during the Faradaic charge storage process. The cycling performance of the $NiCo_2O_4$ electrode is evaluated by the continuous charge–discharge testing at a current density of 5 $A g^{-1}$ and the result is shown in Figure 4D. Impressively, the cycling is very stable with a specific capacitance of 914 $F g^{-1}$ retained over 4000 cycles, corresponding to a loss of only 5.3%. This enhanced cycling stability is probably attributed to the unique core-in-double-shell hollow structure that is expected to improve the structural integrity.

In summary, we have developed a new and efficient strategy for the synthesis of uniform $NiCo_2O_4$ hollow spheres with complex interior structure. This method first involves the synthesis of NiCo-glycerate solid spheres by a simple solvothermal method. Then, the NiCo-glycerate solid spheres can be converted to $NiCo_2O_4$ complex hollow spheres by a simple thermal annealing in air. The formation of the complex interior structure during thermal decomposition of metal glycerate is a result of the combined effect of contraction and adhesion actions caused by non-equilibrium heat treatment. It is further demonstrated that this method is potentially general for the synthesis of metal oxide complex hollow spheres. The resultant $NiCo_2O_4$ hollow spheres possess a unique core-in-double-shell complex interior structure, and the porous shells are constructed by small nanocrystalline particles. As a result, these $NiCo_2O_4$ hollow spheres manifest superior electrochemical performance when evaluated as electrode materials for both lithium-ion batteries and supercapacitors. These uniform metal glycerate spheres can also serve as precursor for the synthesis of other functional materials like metal sulfides.[43]

Received: October 6, 2014
Revised: November 6, 2014
Published online: December 17, 2014

Keywords: Li-ion batteries · mixed metal oxides · nanoparticles · supercapacitors

[1] M. H. Oh, T. Yu, S. H. Yu, B. Lim, K. T. Ko, M. G. Willinger, D. H. Seo, B. H. Kim, M. G. Cho, J. H. Park, K. Kang, Y. E. Sung, N. Pinna, T. Hyeon, *Science* **2013**, *340*, 964.
[2] S. H. Im, U. Y. Jeong, Y. N. Xia, *Nat. Mater.* **2005**, *4*, 671.
[3] X. W. Lou, L. A. Archer, Z. C. Yang, *Adv. Mater.* **2008**, *20*, 3987.
[4] T. Kim, E. Momin, J. Choi, K. Yuan, H. Zaidi, J. Kim, M. Park, N. Lee, M. T. McMahon, A. Quinones-Hinojosa, J. W. M. Bulte, T. Hyeon, A. A. Gilad, *J. Am. Chem. Soc.* **2011**, *133*, 2955.
[5] F. Caruso, R. A. Caruso, H. Mohwald, *Science* **1998**, *282*, 1111.
[6] X. Y. Lai, J. Li, B. A. Korgel, Z. H. Dong, Z. M. Li, F. B. Su, J. A. Du, D. Wang, *Angew. Chem. Int. Ed.* **2011**, *50*, 2738; *Angew. Chem.* **2011**, *123*, 2790.
[7] B. Wang, J. S. Chen, H. B. Wu, Z. Y. Wang, X. W. Lou, *J. Am. Chem. Soc.* **2011**, *133*, 17146.
[8] J. Liu, S. Z. Qiao, S. B. Hartono, G. Q. Lu, *Angew. Chem. Int. Ed.* **2010**, *49*, 4981; *Angew. Chem.* **2010**, *122*, 5101.
[9] Y. D. Yin, R. M. Rioux, C. K. Erdonmez, S. Hughes, G. A. Somorjai, A. P. Alivisatos, *Science* **2004**, *304*, 711.
[10] L. Yu, H. B. Wu, X. W. Lou, *Adv. Mater.* **2013**, *25*, 2296.
[11] H. T. Sun, G. Q. Xin, T. Hu, M. P. Yu, D. L. Shao, X. Sun, J. Lian, *Nat. Commun.* **2014**, *5*, 4526.

[12] J. W. Nai, S. Q. Wang, Y. Bai, L. Guo, *Small* **2013**, *9*, 3147.
[13] L. Zhang, H. B. Wu, S. Madhavi, H. H. Hng, X. W. Lou, *J. Am. Chem. Soc.* **2012**, *134*, 17388.
[14] X. W. Lou, D. Deng, J. Y. Lee, J. Feng, L. A. Archer, *Adv. Mater.* **2008**, *20*, 258.
[15] J. M. Tour, *Nature* **2014**, *512*, 30.
[16] L. Zhou, D. Y. Zhao, X. W. Lou, *Adv. Mater.* **2012**, *24*, 745.
[17] Z. C. Wu, M. Zhang, K. Yu, S. D. Zhang, Y. Xie, *Chem. Eur. J.* **2008**, *14*, 5346.
[18] M. Yang, J. Ma, C. L. Zhang, Z. Z. Yang, Y. F. Lu, *Angew. Chem. Int. Ed.* **2005**, *44*, 6727; *Angew. Chem.* **2005**, *117*, 6885.
[19] J. Liu, H. Xia, D. F. Xue, L. Lu, *J. Am. Chem. Soc.* **2009**, *131*, 12086.
[20] J. Y. Wang, N. L. Yang, H. J. Tang, Z. H. Dong, Q. Jin, M. Yang, D. Kisailus, H. J. Zhao, Z. Y. Tang, D. Wang, *Angew. Chem. Int. Ed.* **2013**, *52*, 6417; *Angew. Chem.* **2013**, *125*, 6545.
[21] G. Q. Zhang, X. W. Lou, *Angew. Chem. Int. Ed.* **2014**, *53*, 9041; *Angew. Chem.* **2014**, *126*, 9187.
[22] H. G. Zhang, Q. S. Zhu, Y. Zhang, Y. Wang, L. Zhao, B. Yu, *Adv. Funct. Mater.* **2007**, *17*, 2766.
[23] H. L. Xu, W. Z. Wang, *Angew. Chem. Int. Ed.* **2007**, *46*, 1489; *Angew. Chem.* **2007**, *119*, 1511.
[24] Y. M. Chiang, *Science* **2010**, *330*, 1485.
[25] T. Brezesinski, J. Wang, S. H. Tolbert, B. Dunn, *Nat. Mater.* **2010**, *9*, 146.
[26] P. Simon, Y. Gogotsi, *Nat. Mater.* **2008**, *7*, 845.
[27] J. R. Miller, P. Simon, *Science* **2008**, *321*, 651.
[28] C. G. Morales-Guio, S. D. Tilley, H. Vrubel, M. Gratzel, X. L. Hu, *Nat. Commun.* **2014**, *5*, 3059.
[29] G. Q. Zhang, L. Yu, H. B. Wu, H. E. Hoster, X. W. Lou, *Adv. Mater.* **2012**, *24*, 4609.
[30] C. Z. Yuan, H. B. Wu, Y. Xie, X. W. Lou, *Angew. Chem. Int. Ed.* **2014**, *53*, 1488; *Angew. Chem.* **2014**, *126*, 1512.
[31] F. Y. Cheng, J. A. Shen, B. Peng, Y. D. Pan, Z. L. Tao, J. Chen, *Nat. Chem.* **2011**, *3*, 79.
[32] L. F. Shen, Q. Che, H. S. Li, X. G. Zhang, *Adv. Funct. Mater.* **2014**, *24*, 2630.
[33] T. Y. Wei, C. H. Chen, H. C. Chien, S. Y. Lu, C. C. Hu, *Adv. Mater.* **2010**, *22*, 347.
[34] J. Zhao, Y. C. Zou, X. X. Zou, T. Y. Bai, Y. P. Liu, R. Q. Gao, D. J. Wang, G. D. Li, *Nanoscale* **2014**, *6*, 7255.
[35] Y. N. NuLi, P. Zhang, Z. P. Guo, H. K. Liu, J. Yang, *Electrochem. Solid-State Lett.* **2008**, *11*, A64.
[36] L. L. Li, Y. Cheah, Y. W. Ko, P. Teh, G. Wee, C. L. Wong, S. J. Peng, M. Srinivasan, *J. Mater. Chem. A* **2013**, *1*, 10935.
[37] J. F. Li, S. L. Xiong, Y. R. Liu, Z. C. Ju, Y. T. Qian, *ACS Appl. Mater. Interfaces* **2013**, *5*, 981.
[38] Y. J. Chen, M. Zhuo, J. W. Deng, Z. Xu, Q. H. Li, T. H. Wang, *J. Mater. Chem. A* **2014**, *2*, 4449.
[39] G. Q. Zhang, X. W. Lou, *Sci. Rep.* **2013**, *3*, 1470.
[40] H. L. Wang, Q. M. Gao, L. Jiang, *Small* **2011**, *7*, 2454.
[41] Q. Lu, Y. P. Chen, W. F. Li, J. G. G. Chen, J. Q. Xiao, F. Jiao, *J. Mater. Chem. A* **2013**, *1*, 2331.
[42] C. Z. Yuan, J. Y. Li, L. R. Hou, J. D. Lin, G. Pang, L. H. Zhang, L. Lian, X. G. Zhang, *RSC Adv.* **2013**, *3*, 18573.
[43] L. F. Shen, L. Yu, H. B. Wu, X. Y. Yu, X. G. Zhang, X. W. Lou, *Nat. Commun.* **2014**, submitted.

